THE JOURNAL OF PHYSICAL CHEMISTRY C

ARTICLE

pubs.acs.org/JPCC

Atomic Oxygen Functionalization of Vertically Aligned Carbon Nanotubes

C. Bittencourt,[†] C. Navio,[†] A. Nicolay,[†] B. Ruelle,[‡] T. Godfroid,[‡] R. Snyders,[†,‡] J.-F. Colomer,[§] M. J. Lagos,[∥] X. Ke,[∥] G. Van Tendeloo,[∥] I. Suarez-Martinez,[⊥] and C. P. Ewels*[,#]

[†]Plasma Surface Interaction Chemistry, University of Mons and [‡]Materia Nova, Belgium

[§]Research Centre in Physics of Matter and Radiation, University of Namur, Belgium

[∥]Electron Microscopy for Material Science, University of Antwerp, Belgium

[⊥]Nanochemistry Research Institute, Curtin University of Technology, Perth, Australia

[#]Institut des Matériaux Jean Rouxel, CNRS UMR6502, Université de Nantes, France

ABSTRACT: Vertically aligned multiwalled carbon nanotubes (v-MWCNTs) are functionalized using atomic oxygen generated in a microwave plasma. X-ray photoelectron spectroscopy depth profile analysis shows that the plasma treatment effectively grafts oxygen exclusively at the v-MWCNT tips. Electron microscopy shows that neither the vertical alignment nor the structure of v-MWCNTs were affected by the plasma treatment. Density functional calculations suggest assignment of XPS C 1s peaks at 286.6 and 287.5 eV, to epoxy and carbonyl functional groups, respectively.

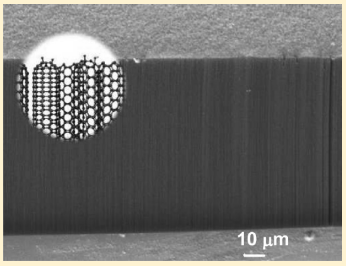

I. INTRODUCTION

Considerable progress has recently been made in the synthesis of vertically aligned carbon nanotubes (v-CNTs), giving rise to a wide range of possible applications including field emission devices, field effect transistors, interconnects, and sensors.[1−5] For example, the metallic character of multiwalled carbon nanotubes (MWCNTs) allows them to promote electron-transfer reactions of proteins at low overpotentials. CNT-functionalized electrodes have been shown to be useful for gathering important biomolecules (e.g., nucleic acids) and for reducing surface fouling effects.[6] The remarkable sensitivity of CNT conductivity to surface interactions along with their large surface area and conformal compatibility with biomolecules provides the grounds for unique biochemical sensing systems.

To take advantage of the outstanding properties of v-CNTs in sensing applications, the surface of the CNT tip needs to be properly functionalized with chemical groups or functional materials to obtain tuned electrical and chemical properties while preserving the intrinsic properties of the v-CNT.[7] In several functionalization strategies, the first step is the grafting of oxygen functional groups; these groups act as active sites for further functionalization.[8] It is impossible to functionalize sp^2 carbon materials at room temperature through exposure to O_2 molecules, due to the high energy barrier that must be overcome to break the covalent oxygen−oxygen bond. Instead, oxygen functionalization is achieved through exposure to atomic oxygen or to strongly oxidizing reactive agents such as a wet solution of strong acids, ozone, or oxygen plasma.[9−15] Acid treatments can extensively damage the structural integrity of the nanotube and exposure to ozone damages the nanotube sidewalls.[16] High energy species such as electrons or ions, often generated in discharge plasmas, can disrupt the CNT skeleton by etching carbon atoms. If the oxidative treatment for grafting the chemical functional groups at the CNT tips extensively damages the tubes, it can compromise their mechanical stability and can then lead to total collapse of the vertically aligned CNTs, subsequently ruling out their use as electrodes.

Several methods such as electrochemical and chemical functionalization, polymer wrapping, mechano-chemical treatment, and plasma treatment have been applied to modify the CNT surface.[17−26] The functionalization of CNTs using a flux of chemical radicals generated in a microwave plasma avoids direct contact of the plasma with the sample surface, reducing the damage caused through etching of carbon atoms. In addition, this technique maintains the advantages of plasma functionalization: it is solvent-free, time-efficient, and flexible, as it can provide a wide range of functional groups depending on the plasma parameters.[27,28] Samples are located in the post-discharge region of the microwave plasma, which is characterized by a high density of chemical radicals and absence of high energy species such as electrons or ions.

In this work, we study the oxygen functionalization of vertically aligned carbon nanotubes using atomic oxygen. The aim is to determine the nature of the resultant functionalization and its spatial distribution, that is, whether the grafting occurs exclusively at the tips of the CNTs. Vertically aligned MWCNTs (v-MWCNTs)

Received: June 20, 2011
Revised: August 25, 2011
Published: September 19, 2011

Table 1. Plasma Parameters Used for the Nanotube Oxygen Treatment[a]

power in the pulse	1600 W
period	800 μs
pulsation time	200 μs
Flow Rate	
argon	75 sccm
oxygen	668 sccm
Pressure	
discharge tube	9.8 Torr
postdischarge chamber	2 Torr

[a] Samples were exposed for either 5 or 30 min.

were synthesized using the thermal catalytic chemical vapor technique. The vertical alignment of the CNTs was observed before and after the treatment using a scanning electron microscope (SEM), and the chemical nature of the grafted functions was evaluated through X-ray photoelectron spectroscopy (XPS). To determine the in-depth distribution and chemical character of the oxygen-radical grafting, the C 1s and O 1s X-ray photoelectron spectra were measured during a depth profiling analysis using a new sputtering tool, buckminsterfullerene (C_{60}) ion sputtering, which has been reported to suppress the degradation of organic and inorganic materials.[29] Spin polarized density functional calculations within the local density approximation (LDA) using the AIMPRO code were performed and used to help interpretation of the XPS data.

II. EXPERIMENTAL SECTION

v-MWCNT Synthesis. v-MWCNTs were synthesized using the conventional thermal catalytic chemical vapor technique (CVD).[30] CNT growth was performed at 750 °C using a mixture of hydrogen and ethylene as the carbon source, and argon was used as a carrier gas. Si wafers (1.5 × 1.5 cm^2) were used as the substrate for the growth of CNTs. An Al_2O_3 layer of 30 nm thickness was used as a buffer layer between the Si substrate and the Fe catalyst layer deposited with a thickness of 6 nm. Both the catalyst and buffer layer were deposited using metal sputtering deposition.

CVD growth was carried out for 30 min as the standard growth time. Upon reaching the growth temperature, a flow of 120 sscm of argon was maintained in the chamber. The substrate was then annealed in an Ar/H_2 mixture (120/130 sscm) for 30 min at the synthesis temperature. After annealing, an ethylene/hydrogen mixture (130/35 sscm) was introduced to synthesize the CNTs.

Sample Functionalization. The CNTs were treated in the postdischarge of an $Ar + O_2$ microwave plasma sustained through a surface wave launched in a quartz tube via a surfaguide supplied by a 2.45 GHz microwave generator whose power maximum is 2 kW and that can be pulsed.[31] This type of plasma processing is suitable to functionalize delicate samples such as the one considered in this work. In this configuration, long-live chemically active radicals is delivered to the so-called post-discharge region that practically does not contain charged heavy particles, nor hot electrons.[32] It has been demonstrated that, for N_2, this plasma configuration allows, when the experimental parameters are optimized, to dissociate up to 43% of N_2 molecules into long-live atomic nitrogen species that can be used for further functionlization in the post-discharge.[31] Since the binding energy of the $\pi-\pi$ covalent bonding in the O_2 molecule is substantially less than the N_2 molecule, respectively, 5.1 and 9.8 eV, it is expected a higher dissociation yield for O_2. Therefore, the O_2 plasma postdischarge likely contains a very high density of atomic oxygen species. The full characterization of the O_2 postdischarge using mass spectrometry and optical emission is an ongoing work. An average distance of 40 cm between the end of the discharge region and the sample holder ensures the nanotubes can only interact with chemical species whose mean lifetime is large enough to reach the tubes. By using this configuration, only atomic species are expected to arrive at the sample surface.[27] The treatment parameters used are presented in Table 1. The samples were functionalized for either 5 or 30 min.

Material Characterization. SEM analyses were performed using an FEI Nova 200 Nanolab dual beam SEM/FIB system. TEM images were acquired using a FEI-Tecnai G20 operated at 200 kV. Imaging process was based on single image acquisition using typical low current density (~15 A/cm^2) and acquisition times of 5 s, which represent a good compromise between obtaining an image with acceptable good signal-to-noise ratio and reducing damage by irradiation.

XPS measurements were performed in a VERSAPROBE PHI 5000 from Physical Electronics, equipped with a monochromatic Al Kα X-ray source with a highly focused beam size that can be set from 10 to 300 μm. The energy resolution was 0.6 eV. For the compensation of the built up charge on the sample surface during the measurements, a dual beam charge neutralization composed of an electron gun (~1 eV) and the argon ion gun ($\leq$10 eV) was used. In XPS depth profiling, the analysis was performed using a C_{60} ion gun operated at 10 keV (20 nA, 2 × 2 mm^2).

The graphite sputtering rate of 0.6 nm/min was evaluated using a SiO_2 reference layer, since the SiO_2 the sputtering rate measured was 1.8 nm/min and the ratio of the calculated Ar sputtering rates for C and SiO_2 is 1:3.

Theoretical Method. We performed spin polarized density functional calculations within the local density approximation (LDA) using the AIMPRO code.[33,34] The LDA has been shown to yield the O_2 binding energy to graphene as well as O_2 singlet/triplet energy differences that are closer to experimental results than that of the generalized gradient approximation.[35] We simulated free edges such as at etched tips or internal defect sites using a graphene ribbon section within a 14.61 × 17.09 × 10.58 $Å^3$ orthogonal supercell that was sufficiently large to avoid interaction between neighboring ribbons. Either a single hydrogen atom on an edge site was replaced with hydroxyl (−OH), carbonyl (=O), carboxylate anion ($-COO^-$), or carboxylic (−COOH) group, or else a single oxygen atom was placed on the middle of the basal plane. The structures were fully geometrically optimized, with a single k-point at ($^1/_2$, $^1/_2$, $^1/_2$). Hartwigsen's, Goedecker's, and Hütter's relativistic pseudopotentials were used for all atoms.[36] Atom-centered Gaussian basis functions were used to construct the many-electron wave function with angular momenta up to $l = 2$ (38 independent functions per C atom, 40 per O, 12 per H). The occupation of the electronic levels was obtained using a Fermi occupation function with kT = 0.04 eV. Charge states were then determined for all atoms in the system using Mulliken population analysis, summing projected orbital populations for each filled electronic level for each atom.

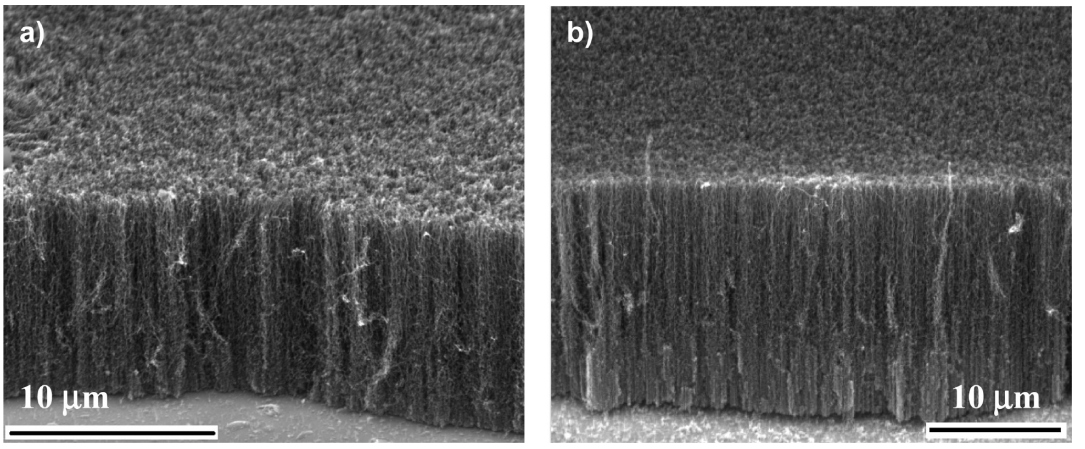

Figure 1. Cross-sectional SEM image of a cleaved CNT film (a) before and (b) after 30 min of functionalization.

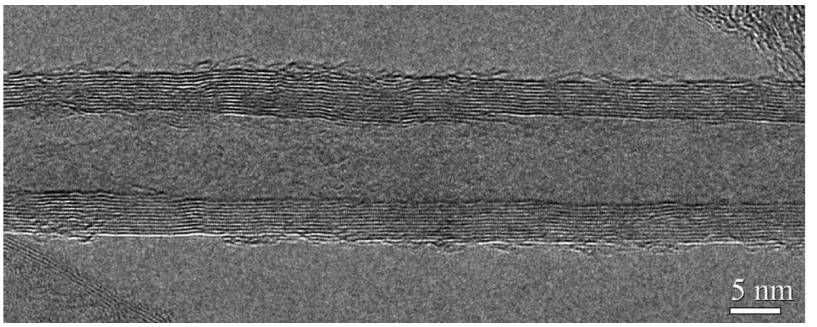

Figure 2. TEM image of a CNT removed from the sample treated for 30 min.

III. RESULTS AND DISCUSSION

Figure 1a shows a SEM image of a cleaved CNT film; a dense and vertically aligned CNT film with average height of 15 μm can be observed. SEM analyses after the functionalization show that the vertical alignment was not affected by the atomic oxygen plasma treatment (Figure 1b). TEM images of individual CNTs removed from the sample treated for 30 min showed that their structure were not affected by the plasma treatment (Figure 2). Nevertheless, few CNTs were found with opened tips (Figure 3). Although, the tips of CNTs were shown to be more reactive than the sidewalls, in most oxidation reactions resulting in the opening of nanotube tips, detrimental damage of their sidewalls also occurs. A close inspection of Figure 3 shows the CNT retained its structural integrity.

Chemical characterization of the samples was performed using XPS. The absence of peaks related to the metal catalysts used for the CNT synthesis in the XPS spectra indicates a base-growth mechanism, that is, the metal catalyst particles remain attached to the underlying substrate. Figure 4 shows the comparison between the C 1s peaks recorded from pristine and atomic oxygen-treated v-MWCNTs and the result of the curve fittings performed to explain the spectra. The pristine C 1s peak is intrinsically asymmetric; this asymmetry is associated with the many-electron response to the sudden creation of a photohole.[37] The associated singularity index α describes the electron−hole interaction, whose strength is reflected in the magnitude of α; the value of the singularity index α can be obtained by fitting the asymmetric C 1s peak with the Doniach−Sunjic (DS) function.[38] By using the

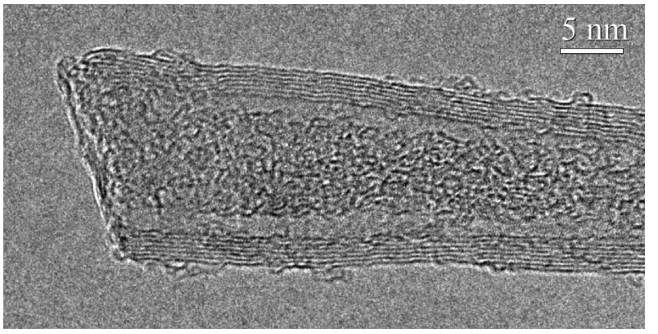

Figure 3. Open CNT found on the sample treated for 30 min. The amorphous carbon at the CNT surface results from the low synthesis temperature.

Doniach−Sunjic function to reproduce the recorded C 1s spectrum, the measured α was 0.15, and the binding energy of the main feature of the spectrum was 284.4 eV. As reported, this feature is generated by photoelectrons emitted from carbon atoms bound to carbon atoms via sp^2 bonds (C═C).[12] In addition to the asymmetric function, two Gaussians were used to reproduce the other features observed in the pristine spectrum. One Gaussian at 285.3 eV is associated with photoelectrons emitted from carbon atoms at sp^3 bonds in amorphous carbon. During CNT nucleation and growth, competing pathways can lead to amorphous carbon formation rather than to crystalline nanotubes; amorphous carbon is reported as one of the main

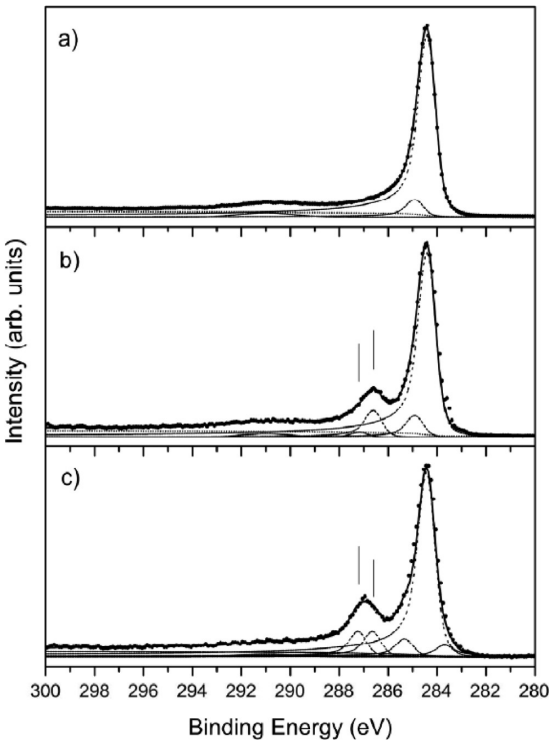

Figure 4. XPS analysis of (a) pristine vertically aligned MWCNTs and oxygen plasma treated MWCNTs for (b) 5 min and (c) 30 min. Vertical lines indicate the components associated with the oxygen functionalization.

by-product in the CVD synthesis of CNTs.[39] The other Gaussian, centered at 291 eV, corresponds to the electron energy loss peak due to π-plasmon excitations.

The chemical modification produced by the atomic oxygen treatment can be identified by a broad structure that peaks at 286.6 eV: this structure was previously attributed to photoelectrons emitted from carbon atoms belonging to carbon functional groups singly and/or doubly bound to one or two oxygen atoms.[40] To reproduce the C 1s peak recorded after 5 min of oxygen functionalization, five components were used: the three components used for fitting the pristine v-MWCNTs and two other Gaussian components, one centered at 286.6 eV and a second at 287.5 eV. In addition to these five components, a component at 283.6 eV was used to reproduce the C1s spectrum for the sample functionalized for 30 min.

As the functionalization time increased, the contribution of the photoelectrons to the relative intensity of these components varied, notably the relative intensity of the peak at 286.6 eV decreased while the intensity of the peak at 287.5 eV increased (see Table 2). This effect suggests that a balance exists between the stability and the reactivity of the grafted groups: at the onset of the oxygen treatment, different chemical groups are grafted, at this stage reactivity would be the principal parameter to define the nature and the amount of the grafted species. Therefore, with increasing treatment time, that is, increasing exposure time to atomic oxygen, variation in the intensity ratio among the components composing the C 1s spectrum is observed. Because the total relative amount of oxygen grafted remained constant (10% inside the volume that can be probed in the XPS analysis), that is, the O/C ratio, we can exclude that the variation in the intensity ratio is related to an increase in the amount of grafted species. Hence, we suggest that the variation in intensity ratio observed for increasing treatment time is due to chemical interaction between the atomic oxygen and the less stable bond configurations.

Table 2. XPS Analysis of the C 1s Peak Recorded on Vertically Aligned MWCNTs as a Function of the Oxygen Plasma Exposure Time (t)

		XPS C 1s peak energy (eV)					
			sp^2	sp^3	π-plasmon		
sample	t (min)	283.6	284.4	285.3	291.0	286.6	287.5
v-MWCNT	0	–	94.4%	2.1%	3.5%	–	–
v-MWCNT	5	–	80.7%	4.2%	2.5%	11.2%	1.4%
v-MWCNT	30	4.3%	68.8%	6.7%	1.6%	9.3%	9.3%

To determine whether the grafting of functional groups takes place mainly at the CNT tips or whether the functionalization extends throughout the CNT walls, an XPS analysis in depth profile was performed. Figure 5 shows the relative intensity of the C 1s and O 1s peaks after a series of sputtering cycles. The relative intensity of the O 1s decreases while the C 1s increases with increasing sputtering time. After the first sputtering cycle, the relative intensity of structures related to carbon atoms bound to oxygen atoms was significantly reduced, indicating the removal of oxygen atoms. The decrease of the O 1s peak intensity after the first sputtering cycle and its complete disappearance after the second sputtering cycle indicates that the functional groups are exclusively grafted at the v-MWCNT tips. We note that, during prolonged sputtering, using a C_{60} ion gun defect creation and deposition of amorphous carbon at the CNT surface might occur.

Interpretation of the C 1s XPS peaks associated with oxygen presence is not trivial. Multiple inconsistent assignments are given in the literature, often without justification, and additionally some authors find peak positions to be a function of oxygen concentration.[41−46] A common assumption is that increasing peak energy implies a signal from a carbon atom with increasing number of C−O bonds, since such an atom should be increasingly positive.[44] To test this hypothesis, we calculated the charge states on carbon atoms depending on the oxygen-related functional groups present, via a series of density functional calculations. Since the nanotubes are large in diameter, we assume surface curvature effects are negligible. We have therefore modeled a section of hydrogen-terminated, zigzag-edge graphene ribbon, where the ribbon edge is used to simulate open nanotube tips or exposed bond sites at defects. We then replaced one −H group with a hydroxyl (−OH), carbonyl (=O), carboxylate anion ($-COO^-$), or carboxylic (−COOH) group. Alternatively, we placed a single O atom above the center of the ribbon, generating an epoxide group. All structures were fully geometrically optimized.

The results are given in Table 3. The functional groups form three broad groups: the most positive is associated with the carboxylic group, followed by the hydroxyl, and then the others give similar values. While in general this follows the "common wisdom" trend based on assignments for small molecules, the exception is the hydroxyl group, which is normally expected to have significantly less carbon polarization.

If we examine the location of the most positive carbon atoms, for both the carboxylic and hydroxyl groups, they are the carbon

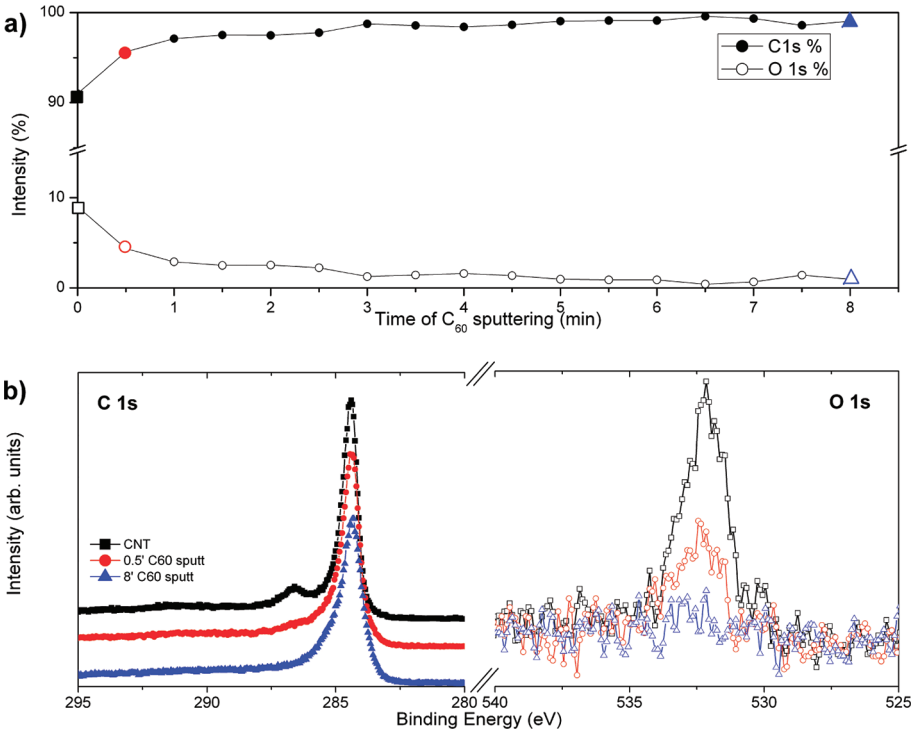

Figure 5. (a) Relative intensity of the O 1s and C 1s peaks measured during the depth profile experiment. (b) Comparison of the spectra recorded after the first (circle) and the last sputtering cycle (triangle) with the spectra recorded before the sputtering (square).

Table 3. Calculated Charge States of Carbon Atoms in a Zigzag Hydrogen-Terminated Graphene Ribbon, with Different Functional Groups Attached Either at a Ribbon Edge Site or to the Basal Plane (Epoxide)[a]

atom	—O— epoxy	>C—COO^- carboxylate anion	>C═O carbonyl	>C—OH hydroxyl	>C—COOH carboxylic
most positive carbon	+0.167	+0.172	+0.190	+0.269	+0.371
	NN	–	–	*F*	*F*
most negative carbon	−0.129	−0.094	−0.112	−0.077	−0.050
	–	–	–	–	–

[a] The location of the most positive carbon atom in the system is indicated by the following: *F* (within the functional group itself), *NN* (nearest neighbour to the functional group), or – (elsewhere in the system).

atoms attached to or forming part of the functional group. In the case of the carbonyl and carboxylate anion, the most positive carbon atoms are elsewhere. Finally, for the epoxide, surprisingly, the C atoms attached directly to the oxygen are not strongly positive, and instead, it is their neighbors that have the highest positive charge. Charge distribution for key structures is shown in Figure 6. We conclude that the principle of the C 1s peak assignment to oxygen functionalized groups based on an assumption of increasingly positive carbon atom within the functional group with increasing C−O bonds needs revisiting.

An alternative approach sometimes used for the theoretical assignment of core shifts energies is via the equivalent core (Z + 1) approach, comparing total system energies when a given atom is replaced by an atom with an additional proton, simulating the loss of a core electron.[47] Once again, the current charge state comparison calculations suggest that the correct way to implement this is via core shift calculations for all atoms showing changing charge states, rather than just atoms neighboring the oxygen impurity. Such calculations are beyond the scope of the current article but will be the subject of a later study.

We tentatively assign the observed C 1s XPS peaks based on our calculations, although we appreciate that atom charge is only one of several factors governing XPS peak position. The least shifted peak from the C 1s sp^2 peak lies at 286.6 eV, and we therefore assign this to the oxygen defect associated with the least positive carbon atoms, the epoxide unit. By the same logic the next peak at 287.5 eV is therefore assigned to carbonyl groups. Peak assignments from detailed core−electron removal calculations in the literature are broadly similar to this with some exceptions, although they consider a wider range of defect types.[48] However, those literature calculations involve excitations of a C 1s core electron, and while not specified, we assume this is from a carbon atom neighboring the oxygen centers; again in light of our results, transitions from other carbon atoms may need to be incorporated as well.

These assignments aid the interpretation of the experimental results. For the v-MWCNTs, after 5 min of oxygen treatment, the presence of epoxide groups is observed. This will be associated with epoxide oxygen addition to the basal plane, and notably facet edges on large polygonal tips (since epoxide addition to regions

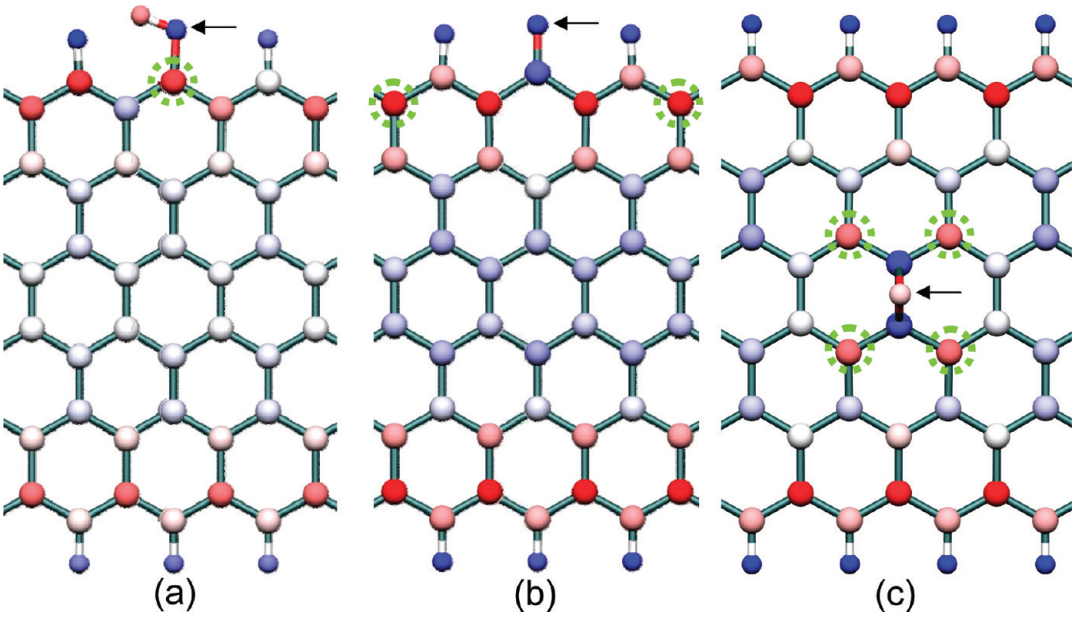

Figure 6. Calculated charge distribution for (a) hydroxyl (C—OH), (b) carbonyl (C═O), and (c) central epoxy groups showing that the most positive carbon atoms in the system are not always those of the functional group itself. Darker blue (red) = more negative (positive). Green dotted circles enclose the most positive carbon atoms in the system, excluding those associated with the edge in (c). Arrow indicates oxygen atom (color online).

with curvature is more exothermic.[49] Oxygen atom addition to the basal plane is exothermic (for our graphene ribbon, we calculate a binding energy of 3.47 eV, in good agreement with a literature value of 3.23 eV).[50] However, it is nonetheless endothermic as compared to the isolated ribbon and $^1/_2$ O_2, by 0.52 eV. This constrains the maximum epoxide concentration, since although individual oxygen atoms will bind to the tube, a second oxygen atom impact in the same area will bond to the first, releasing O_2 (1.04 eV). In addition, oxygen surface migration can also lead to recombination.

Over a long period of time, the peak associated with carbonyls increases, consistent with the observation that the tips are gradually being opened, the resultant dangling bonds being terminated by oxygen atoms.

IV. CONCLUSION

Vertically aligned multiwalled carbon nanotubes (v-MWCNTs) can be functionalized using atomic oxygen generated in a microwave plasma. XPS analysis supported by density functional calculations shows the grafting of epoxy and carbonyl functional groups. XPS depth profile analysis showed that the plasma treatment effectively grafts oxygen exclusively at the v-MWCNT tips. Initial oxidation is via epoxide surface groups bonding to the tip (probably along tip facets), but with time, the tips are chemically opened and the carbon dangling bond sites terminated with carbonyl groups. By tuning the oxidation time, it is possible to preferentially obtain epoxide or carbonyl enriched tube tips.

AUTHOR INFORMATION

Corresponding Author

*Fax: +33-240373998. E-mail: chris.ewels@cnrs-imn.fr.

ACKNOWLEDGMENT

This work is partially supported by the European Commission under contract ERC 246791 (COUNTATOMS), Belgian Program on Interuniversity Attraction Pole (PAI 6/08) and ARC-UMONS. C.P.E. acknowledges the NANOSIM-GRAPHENE project no. ANR-09-NANO-016-01 funded by the French National Agency (ANR) in the frame of its 2009 programme in Nanosciences, Nanotechnologies & Nanosystems (P3N2009). We thank Ms. Ramona Shelby for her careful revision in English. The support of the COST Action MP0901 "NanoTP" is gratefully acknowledged.

REFERENCES

(1) Postma, H. W. C.; Teepen, T.; Yao, Z.; Grifoni, M.; Dekker, C. *Science* **2001**, *293*, 76.
(2) Fan, S. S.; Chapline, M. G.; Franklin, N. R.; Tombler, T. W.; Cassell, A. M.; Dai, H. J. *Science* **1999**, *283*, 512.
(3) Lim, S. C.; Jang, J. H.; Bae, D. J.; Han, G. H.; Lee, S.; Yeo, I. S.; Lee, Y. H. *Appl. Phys. Lett.* **2009**, *95*, 264103 .
(4) Burghard, M. *Small* **2005**, *1*, 1148.
(5) Roy, S.; Vedala, H.; Choi, W. *Nanotechnology* **2006**, *17*, S14.
(6) Wang, J.; Kawde, A. N.; Musameh, M. *Analyst* **2003**, *128*, 912.
(7) Marega, R.; Aroulmoji, V.; Dinon, F.; Vaccari, L.; Giordani, S.; Bianco, A.; Murano, E.; Prato, M. *J. Am. Chem. Soc.* **2009**, *131*, 9086.
(8) Cellot, G.; Cilia, E.; Cipollone, S.; Rancic, V.; Sucapane, A.; Giordani, S.; Gambazzi, L.; Markram, H.; Grandolfo, M.; Scaini, D.; Gelain, F.; Casalis, L.; Prato, M.; Giugliano, M.; Ballerini, L. *Nat. Nanotechnol.* **2009**, *4*, 126.
(9) Goldoni, A.; Larciprete, R.; Petaccia, L.; Lizzit, S. *J. Am. Chem. Soc.* **2003**, *125*, 11329.
(10) Ulbricht, H.; Moos, G.; Hertel, T. *Phys. Rev. B: Condens. Matter Mater. Phys.* **2002**, *66*, 075404/1.
(11) Larciprete, R.; Gardonio, S.; Petaccia, L.; Lizzit, S. *Carbon* **2009**, *47*, 2579.
(12) Barinov, A.; Gregoratti, L.; Dudin, P.; La Rosa, S.; Kiskinova, M. *Adv. Mater.* **2009**, *21*, 1916.
(13) Zielke, U.; Huttinger, K. J.; Hoffman, W. P. *Carbon* **1996**, *34*, 983.
(14) Mawhinney, D. B.; Naumenko, V.; Kuznetsova, A.; Yates, J. T.; Liu, J.; Smalley, R. E. *J. Am. Chem. Soc.* **2000**, *122*, 2383.
(15) Ago, H.; Kugler, T.; Cacialli, F.; Salaneck, W. R.; Shaffer, M. S. P.; Windle, A. H.; Friend, R. H. *J. Phys. Chem. B* **1999**, *103*, 8116.

(16) Simmons, J. M.; Nichols, B. M.; Baker, S. E.; Marcus, M. S.; Castellini, O. M.; Lee, C. S.; Hamers, R. J.; Eriksson, M. A. *J. Phys. Chem. B* **2006**, *110*, 7113.
(17) Bahr, J. L.; Yang, J. P.; Kosynkin, D. V.; Bronikowski, M. J.; Smalley, R. E.; Tour, J. M. *J. Am. Chem. Soc.* **2001**, *123*, 6536.
(18) Cao, L.; Chen, H. Z.; Wang, M.; Sun, J. Z.; Zhang, X. B.; Kong, F. Z. *J. Phys. Chem. B* **2002**, *106*, 8971.
(19) Tasis, D.; Tagmatarchis, N.; Georgakilas, V.; Prato, M. *Chem.—Eur. J.* **2003**, *9*, 4001.
(20) Dettlaff-Weglikowska, U.; Benoit, J. M.; Chiu, P. W.; Graupner, R.; Lebedkin, S.; Roth, S. *Curr. Appl. Phys.* **2002**, *2*, 497.
(21) O'Connell, M. J.; Boul, P.; Ericson, L. M.; Huffman, C.; Wang, Y. H.; Haroz, E.; Kuper, C.; Tour, J.; Ausman, K. D.; Smalley, R. E. *Chem. Phys. Lett.* **2001**, *342*, 265.
(22) Konya, Z.; Vesselenyi, I.; Niesz, K.; Kukovecz, A.; Demortier, A.; Fonseca, A.; Delhalle, J.; Mekhalif, Z.; Nagy, J. B.; Koos, A. A.; Osvath, Z.; Kocsonya, A.; Biro, L. P.; Kiricsi, I. *Chem. Phys. Lett.* **2002**, *360*, 429.
(23) Chen, Q. D.; Dai, L. M.; Gao, M.; Huang, S. M.; Mau, A. *J. Phys. Chem. B* **2001**, *105*, 618.
(24) Shi, D. L.; Lian, J.; He, P.; Wang, L. M.; van Ooij, W. J.; Schulz, M.; Liu, Y. J.; Mast, D. B. *Appl. Phys. Lett.* **2002**, *81*, 5216.
(25) Bubert, H.; Haiber, S.; Brandl, W.; Marginean, G.; Heintze, M.; Bruser, V. *Diamond Relat. Mater.* **2003**, *12*, 811.
(26) Plank, N. O. V.; Jiang, L. D.; Cheung, R. *Appl. Phys. Lett.* **2003**, *83*, 2426.
(27) Ruelle, B.; Peeterbroeck, S.; Gouttebaron, R.; Godfroid, T.; Monteverde, F.; Dauchot, J. P.; Alexandre, M.; Hecq, M.; Dubois, P. *J. Mater. Chem.* **2007**, *17*, 157.
(28) Ruelle, B.; Felten, A.; Ghijsen, J.; Drube, W.; Johnson, R. L.; Duoduo, L.; Erni, R.; Van Tendeloo, G.; Dubois, P.; Hecq, M.; Bittencourt, C. *J. Phys. D: Appl. Phys.* **2008**, 045202.
(29) Fisher, G. L.; Dickinson, M.; Bryan, S. R.; Moulder, J. *Appl. Surf. Sci.* **2008**, *255*, 819.
(30) Chhowalla, M.; Ducati, C.; Rupesinghe, N. L.; Teo, K. B. K.; Amaratunga, G. A. J. *Appl. Phys. Lett.* **2001**, *79*, 2079.
(31) Godfroid, T.; Dauchot, J. P.; Hecq, M. *Surf. Coat. Technol.* **2003**, *174*, 1276.
(32) Merel, P.; Tabbal, M.; Chaker, M.; Moisan, M.; Ricard, A. *Plasma Sources Sci. Technol.* **1998**, *7*, 550.
(33) Briddon, P. R.; Jones, R. *Phys. Status Solidi B* **2000**, *217*, 131.
(34) Rayson, M. J.; Briddon, P. R. *Comput. Phys. Commun.* **2008**, *178*, 128.
(35) Giannozzi, P.; Car, R.; Scoles, G. *J. Chem. Phys.* **2003**, *118*, 1003.
(36) Hartwigsen, C.; Goedecker, S.; Hutter, J. *Phys. Rev. B* **1998**, *58*, 3641.
(37) Hufner, S. *Photoelectron Spectroscopy*; Springer-Verlag: New York, 2003.
(38) Doniach, S.; Sunjic, M. *J. Phys. C: Solid State Phys.* **1970**, *3*, 285.
(39) Nessim, G. D.; Hart, A. J.; Kim, J. S.; Acquaviva, D.; Oh, J. H.; Morgan, C. D.; Seita, M.; Leib, J. S.; Thompson, C. V. *Nano Lett.* **2008**, *8*, 3587.
(40) Okpalugo, T. I. T.; Papakonstantinou, P.; Murphy, H.; McLaughlin, J.; Brown, N. M. D. *Carbon* **2005**, *43*, 153.
(41) Nikitin, A.; Ogasawara, H.; Mann, D.; Denecke, R.; Zhang, Z.; Dai, H.; Cho, K.; Nilsson, A. *Phys. Rev. Lett.* **2005**, *95*, 225507/1.
(42) Desimoni, E.; Casella, G. I.; Morone, A.; Salvi, A. M. *Surf. Interface Anal.* **1990**, *15*, 627.
(43) Szabo, T.; Berkesi, O.; Forgo, P.; Josepovits, K.; Sanakis, Y.; Petridis, D.; Dekany, I. *Chem. Mater.* **2006**, *18*, 2740.
(44) Jeong, H. K.; Colakerol, L.; Jin, M. H.; Glans, P. A.; Smith, K. E.; Lee, Y. H. *Chem. Phys. Lett.* **2008**, *460*, 499.
(45) Jeong, H. K.; Lee, Y. P.; Lahaye, R.; Park, M. H.; An, K. H.; Kim, I. J.; Yang, C. W.; Park, C. Y.; Ruoff, R. S.; Lee, Y. H. *J. Am. Chem. Soc.* **2008**, *130*, 1362.
(46) Xie, Y. M.; Sherwood, P. M. A. *Chem. Mater.* **1990**, *2*, 293.
(47) Martensson, N.; Johansson, B. *Solid State Commun.* **1979**, *32*, 791.
(48) Zhang, W. H.; Carravetta, V.; Li, Z. Y.; Luo, Y.; Yang, J. L. *J. Chem. Phys.* **2009**, *131*, 244505 .
(49) Suarez-Martinez, I.; Ewels, C. P.; Monthioux, M. **2011**, submitted for publication.
(50) Lee, G.; Lee, B.; Kim, J.; Cho, K. *J. Phys. Chem. C* **2009**, *113*, 14225.